Neuron, Vol. 37, 221–231, January 23, 2003, Copyright ©2003 by Cell Press

Axonal Targeting of Olfactory Receptor Neurons in *Drosophila* Is Controlled by Dscam

Thomas Hummel,[1,3] Maria Luisa Vasconcelos,[1,3] James C. Clemens,[1] Yelena Fishilevich,[2] Leslie B. Vosshall,[2] and S. Lawrence Zipursky[1,*]
[1]Howard Hughes Medical Institute
Department of Biological Chemistry
The David Geffen School of Medicine at UCLA
Los Angeles, California 90095
[2]Laboratory of Neurogenetics
The Rockefeller University
New York, New York 10021

Summary

Different classes of olfactory receptor neurons (ORNs) in *Drosophila* innervate distinct targets, or glomeruli, in the antennal lobe of the brain. Here we demonstrate that specific ORN classes require the cell surface protein Dscam (Down Syndrome Cell Adhesion Molecule) to synapse in the correct glomeruli. *Dscam* mutant ORNs frequently terminated in ectopic sites both within and outside the antennal lobe. The morphology of Dscam mutant axon terminals in either ectopic or cognate targets was abnormal. Target specificity for other ORNs was not altered in *Dscam* mutants, suggesting that different ORNs use different strategies to regulate wiring. Multiple forms of Dscam RNA were detected in the developing antenna, and Dscam protein was localized to developing ORN axons. We propose a role for Dscam protein diversity in regulating ORN target specificity.

Introduction

The molecular basis of target specificity underlying synaptic circuitry remains a central issue in neurobiology. Neurons form connections in a stepwise fashion (Tessier-Lavigne and Goodman, 1996). They extend axons along stereotyped pathways toward their targets responding to and integrating multiple short- and long-range guidance signals that attract or repel growth cones (Yu and Bargmann, 2001). Once within the target region, axons form synapses with specific cells. Given the extraordinary complexity of neuronal connectivity, it seems likely that a variety of molecular strategies have evolved to control target specificity, including gradients of recognition molecules (Flanagan and Vanderhaeghen, 1998) and combinations of different signals and growth cone receptors (Winberg et al., 1998). Families of related cell surface molecules with different recognition properties have also been proposed to play critical roles in controlling target specificity. Indeed, extensive molecular diversity among families of cell surface proteins does exist within the nervous system, and some of these proteins may contribute to specificity. In the vertebrate olfactory system, for example, a thousand or so odorant receptors regulate targeting of olfactory receptor neurons to specific glomeruli in the olfactory bulb (Mombaerts et al., 1996; Wang et al., 1998). The role of other diverse families of receptors in regulating target specificity, including cadherin-related neuronal receptors (Kohmura et al., 1998; Wu and Maniatis, 1999) and MHC class I molecules (Huh et al., 2000), remains poorly understood.

In *Drosophila*, there is at least one family of highly related axon guidance receptors encoded by the *Dscam* locus. Dscam is a cell surface molecule of the immunoglobulin (Ig) superfamily (Schmucker et al., 2000; Yamakawa et al., 1998). As many as 38,016 isoforms of Dscam may be generated by alternative splicing of transcripts from a single gene (Schmucker et al., 2000). Dscam isoforms share an identical domain structure with ten Ig and six fibronectin type III repeats, a single transmembrane domain, and a cytoplasmic tail. They have different combinations of variable Ig2, Ig3, and Ig7 domains and one of two alternative transmembrane segments (see Figure 1I below). The existence of many forms of Dscam raises the intriguing prospect that they contribute to the recognition mechanisms underlying the selection of specific synaptic targets.

Previous studies revealed that Dscam is required for axon guidance (Schmucker et al., 2000; Wang et al., 2002). In the embryonic nervous system, Dscam is proposed to promote interactions between Bolwig's nerve growth cones and an intermediate target. In the post-embryonic nervous system, Wang et al. (2002) demonstrated that mushroom body neurons form primary axon branches as in wild-type but that these frequently migrate along inappropriate pathways and exhibit excessive branching in terminal regions. They also showed that neurons in the ellipsoid body exhibit abnormal terminal morphologies. These systems are not amenable to assessing whether Dscam is required for target specificity, as either appropriate markers are not available or, alternatively, defects at earlier stages of axon guidance preclude assessment of Dscam's role in targeting. Accordingly, we sought to assess targeting in the olfactory system, as there are markers for different classes of neurons that exhibit different targeting specificities.

Drosophila olfactory receptor neurons (ORNs) are located in two adult appendages, the third segment of the antenna and the maxillary palps of the proboscis (Stocker et al., 1990; see Figures 1A and 1B). In the antenna, there are approximately 35 OR genes expressed in 1200 ORNs (Clyne et al., 1999; Vosshall et al., 1999; Gao and Chess, 1999) that converge upon about 35 glomeruli (see Laissue et al., 1999). Therefore, it is likely that each subclass of ORNs expressing a given OR gene occupies a unique and dedicated glomerulus. In contrast, ORNs from the maxillary palps (120 ORNs in at least eight classes) show some level of coconvergence to a smaller number of glomeruli (Gao et al., 2000; Vosshall et al., 2000; Y.F. and L.B.V., unpublished data). Within glomeruli, ORNs make synaptic connections with dendrites of projection neurons (Stocker et al., 1990). As there is no simple topographic relationship in flies

*Correspondence: zipursky@hhmi.ucla.edu
[3]These authors contributed equally to this work.

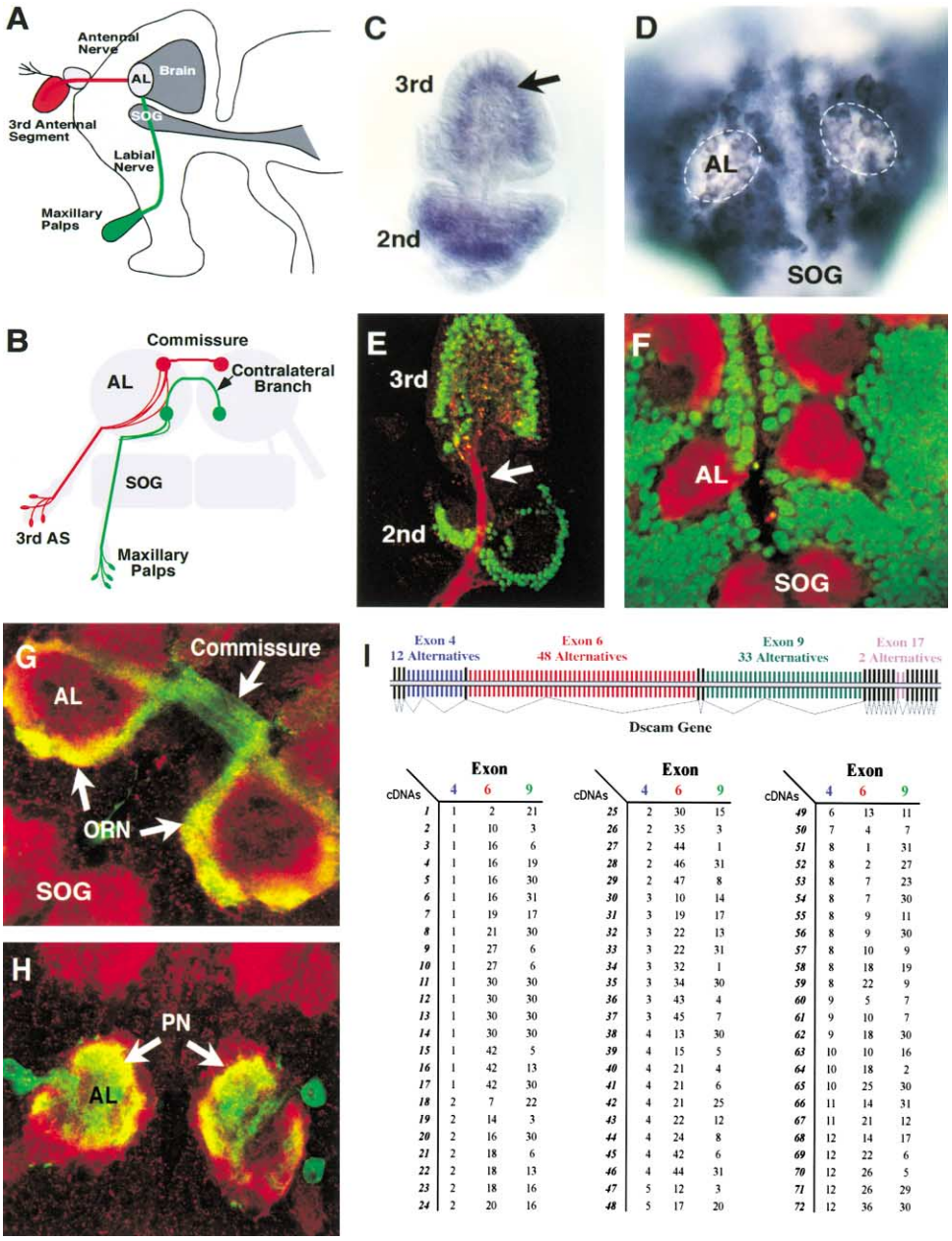

cDNAs	Exon 4	Exon 6	Exon 9
1	1	2	21
2	1	10	3
3	1	16	6
4	1	16	19
5	1	16	30
6	1	16	31
7	1	19	17
8	1	21	30
9	1	27	6
10	1	27	6
11	1	30	30
12	1	30	30
13	1	30	30
14	1	30	30
15	1	42	5
16	1	42	13
17	1	42	30
18	2	7	22
19	2	14	3
20	2	16	30
21	2	18	6
22	2	18	13
23	2	18	16
24	2	20	16
25	2	30	15
26	2	35	3
27	2	44	1
28	2	46	31
29	2	47	8
30	3	10	14
31	3	19	17
32	3	22	13
33	3	22	31
34	3	32	1
35	3	34	30
36	3	43	4
37	3	45	7
38	4	13	30
39	4	15	5
40	4	21	4
41	4	21	6
42	4	21	25
43	4	22	12
44	4	24	8
45	4	42	6
46	4	44	31
47	5	12	3
48	5	17	20
49	6	13	11
50	7	4	7
51	8	1	31
52	8	2	27
53	8	7	23
54	8	7	30
55	8	9	11
56	8	9	30
57	8	10	9
58	8	18	19
59	8	22	9
60	9	5	7
61	9	10	7
62	9	18	30
63	10	10	16
64	10	18	2
65	10	25	30
66	11	14	31
67	11	21	12
68	12	14	17
69	12	22	6
70	12	26	5
71	12	26	29
72	12	36	30

Figure 1. Dscam Is Expressed in the Olfactory System

(A) The cell bodies of olfactory receptor neurons (ORNs) are located in the third antennal segment and the maxillary palps.

(B) ORNs in the third antennal segment project along the antennal nerve into the antennal lobe (AL). ORNs from the maxillary palps project along the labial nerve through the suboesophageal ganglion (SOG) and into the antennal lobe. Different classes of ORNs target to different synaptic units called glomeruli (red and green circles). Most classes of ORNs extend a branch to a symmetric glomerulus on the contralateral side.

(C–H) The expression of Dscam in the olfactory system at about 30% pupal development as ORNs project into the antennal lobe. (C) Dscam RNA is expressed in the third antennal segment (containing ORNs, arrow) as well as in the second antennal segment (containing mechanosensory neurons). (D) In the CNS, Dscam RNA is expressed in target neurons surrounding the antennal lobe. (E) Dscam protein detected with a C-terminally directed antibody (red) is expressed on axons projecting into the antennal nerve (arrow). Note that little staining is seen in neuronal cell bodies (neuronal nuclei highlighted by staining in green with anti-Elav). (F) Dscam protein (red) is localized to neuropil of the AL as well as the SOG. Note staining is highly neuropil specific with little expression detected in the surrounding cortical region (anti-Elav, green). (G and H) Dscam protein is expressed on processes of both ORNs and target neurons. (G) ORNs are visualized by expression of UAS-mCD8-GFP driven by elav-Gal 4 (green). elav-Gal4 is active selectively in ORNs as expression in target neurons is prevented by coexpression of Gal80. Gal80 has been removed selectively from the antenna using *eyeless-FLP* (see text and Figure 2). Intense Dscam staining in the center of the neuropil is associated with processes of target cells (red). (H) Staining of the processes of projection neurons is visualized using the enhancer trap GH146-Gal4 to drive expression of UAS-mCD8-GFP (green).

(I) Many different isoforms of Dscam are expressed in the developing antenna (~30% pupal development). Multiple forms of Dscam are generated by alternative splicing. Alternative exons 4 and 6 encode variable sequences of the first half of Ig domains 2 and 3, alternative

between the position of ORNs in the periphery and the location of the target glomerulus in the antennal lobe (Vosshall et al., 2000), it seems likely that specificity is determined by molecular labels that specify point-to-point mapping. In contrast to vertebrate systems, odorant receptors in flies are expressed after the formation of glomeruli (Clyne et al., 1999; Elmore and Smith, 2001), and hence, it is unlikely that they play a role in targeting similar to that in the mouse olfactory system. Here we show that Dscam plays a crucial role in the targeting of a subset of ORNs.

Results

Dscam Is Expressed in Olfactory Receptor Neurons

Dscam expression was assessed in the developing olfactory system using both in situ hybridization and immunohistology (Figure 1). Between 30% to 40% of pupal development, Dscam RNA was seen in the third antennal segment that contains differentiating ORNs (Figure 1C). At this stage of development, many ORNs extend axons into the antennal lobe. Within the target region, Dscam RNA was observed in most, and perhaps all, neuronal cell bodies surrounding the antennal lobe; this region includes the cell bodies of both projection neurons and local interneurons (Figure 1D). Dscam protein was highly enriched in ORN axons in early to mid pupal development, with little immunoreactivity apparent on cell bodies, as assessed using an antibody directed to a domain shared by all Dscam isoforms (Figure 1E). Similarly, little Dscam immunoreactivity was observed on cell bodies of interneurons and projection neurons (Figure 1F). At 40% pupal development, Dscam protein was seen on ORN axons in the peripheral nerve fiber layer surrounding the developing antennal lobe (Figure 1G). Dscam was also detected on the centrally located dendritic processes of antennal lobe neurons (e.g., projection neurons [PN] in Figure 1H). At later stages, Dscam immunoreactivity was seen uniformly distributed within developing glomeruli and was markedly downregulated in the antennal lobe of adult flies (data not shown). In contrast to the vertebrate olfactory system, ORNs in flies are not generated throughout the life of the animal, and hence, it would not be surprising that genes that regulate targeting in the fly olfactory system would be downregulated in the adult.

To assess the diversity of Dscam isoforms expressed in the developing ORNs, we isolated third antennal segments at 30% pupal development and analyzed the RNA isoforms expressed using RT-PCR (Schmucker et al., 2000). Seventy-two different clones from six different antennae were sequenced, and sixty-eight of these comprised different combinations of alternative exons 4, 6, and 9 (encoding amino acids in Ig2, Ig3, and Ig7, respectively) (Figure 1I). No striking preferential patterns of alternative exon utilization or combinations of exons were apparent. While Dscam protein is largely expressed in ORNs at this stage, we cannot rule out the possibility that Dscam RNA but not protein is expressed in other cells. As markers for different subclasses of ORNs are expressed after glomeruli are formed, it has not yet been possible to assess the forms of Dscam expressed in different subclasses of ORNs as they target to specific glomeruli. Nevertheless, these data are consistent with many different forms of Dscam protein being produced by ORNs as they project into the target region and that individual ORNs express multiple Dscam isoforms.

Dscam Is Not Required in Antennal ORNs for Axon Guidance

As *Dscam* strong loss-of-function alleles are embryonic lethal, we used the MARCM technique (Lee and Luo, 1999; Figure 2A) to assess the function of Dscam in ORNs. The eyeless (ey) promoter drives expression of FLP recombinase (ey-FLP) in the developing antennae and maxillary palps and produces large clones of *Dscam* mutant ORNs (Figures 2B and 2C). Importantly, ey-FLP does not drive mitotic recombination in the target cells (Figure 2D). The phenotypes associated with three *Dscam* alleles ($Dscam^{21}$, $Dscam^{23}$, and $Dscam^{33}$) were analyzed. Protein was not detected in these alleles with either N- or C-terminally directed antibodies. As the phenotypes observed in embryos carrying any one of these alleles rendered hemizygous in *trans* to a deficiency were not appreciably stronger than in homozygotes, we define them as strong loss-of-function alleles. All three alleles gave rise to similar phenotypes in the embryo as well as in the mushroom bodies, the visual system (data not shown), and the olfactory system (see below). As $Dscam^{21}$, in some contexts, exhibited stronger phenotypes, residual activity may be present in $Dscam^{23}$ and $Dscam^{33}$.

The projections of wild-type and mutant ORNs were visualized using expression UAS-nCD8-GFP under the control of a pan-neuronal driver, elav-Gal4 (Figures 2D–2G). *Dscam* mutant ORNs from the antenna projected through the antennal nerve into the antennal lobe in a manner largely indistinguishable from wild-type (Figures 2D and 2E). The fiber patterns of mutant ORNs along the periphery of the antennal lobe appeared normal (data not shown). At higher magnification (Figures 2F and 2G), however, differences between wild-type and mutant were apparent in the pattern of termini in more central regions of the antennal lobe. While wild-type axons elaborated processes that extend throughout glomeruli, *Dscam* mutant axons frequently formed discrete dense aggregates (Figure 2G, arrows). The morphology of glomeruli, as assessed with the neuropil marker nc82, appeared normal (data not shown). Hence, axon guidance of antennal ORNs to the target, the antennal lobe, is indistinguishable from wild-type; *Dscam* mutations appear to affect ORN development once the fibers are within the target region. In contrast to *Dscam* mutant antennal ORNs, maxillary palp mutant ORN axons that

exon 9 encodes Ig domain 7, and there are two alternative transmembrane domains encoded by variable exons 17. Seventy-two different cDNAs were isolated from RT-PCR reactions from total RNA isolated from six different antennae at 30% development and sequenced. The combinations of different alternative exons 4, 6, and 9 are shown. Both alternative exons 17.1 and 17.2 are also expressed (data not shown).

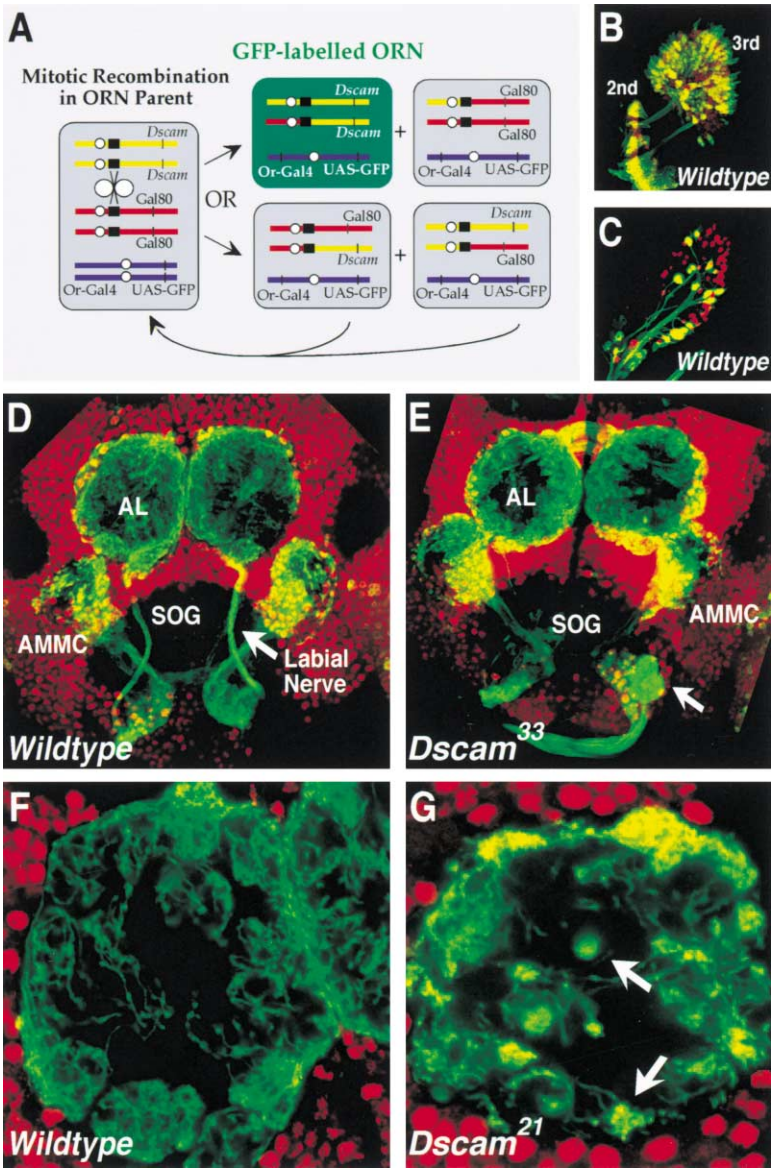

Figure 2. ORNs from the Antenna and Maxillary Palps Visualized by the MARCM Technique

(A) The role of Dscam in ORN targeting was assessed using the MARCM technique (Lee and Luo, 1999). Flies heterozygous for *Dscam* mutations were generated. The homologous chromosome arm carried a transgene expressing Gal80 under a constitutive promoter. Mitotic recombination was generated between FRT sites by FLP recombinase expressed under the eyeless promoter (ey-FLP), which drives expression in ORN precursors, but not in target neurons. In other experiments (i.e., in Figure 5), FLP was expressed under heat shock control to give small clones. Mutant clones were visualized by expression of UAS-mCD8-GFP or UAS-nsyb-GFP (e.g., see Figure 3) to visualize axons or synaptic terminals, respectively. In this figure, expression was driven in all ORNs by Gal4 under the elav-promoter. In other experiments, mutant ORNs express GFP under the control of promoters from specific odorant receptors that are expressed in neurons that target to the same glomerulus (e.g., see Figure 3).

(B–D) Wild-type animals. ey-FLP induces labeling in ORNs in the third antennal segments (B) and maxillary palps (C) but not in antennal lobe target cells. There are no yellow cells in single optical sections (see [F] and [G]). Yellow-appearing cells result from the merging of multiple optical sections. (D) Wild-type labeled fibers from the antenna and maxillary palps project into the antennal lobe neuropil along the antennal nerve (not shown) and along the labial nerve (arrow), respectively. Mechanosensory neurons from both the second antennal segment and the maxillary palps project into the antenna mechanosensory motor center (AMMC).

(E) The overall innervation pattern of *Dscam* mutant ORNs projecting into the antennal lobe from the antenna is largely normal. Due to the relative orientation of panels (D) and (E), the commissure looks expanded (arrowhead), and fibers appear to extend beyond the normal confines of the antennal lobe. Frequently, axons from ORNs in the maxillary palps terminate in clusters prior to entering the antennal lobe (arrow; see text and Figure 6).

(F and G) High-magnification views of the antennal lobe neuropil innervated by wild-type (F) and *Dscam* mutant (G) fibers. All mutant but no wild-type fibers in these preparations are labeled. About 50% of all ORNs are mutant. Wild-type ORNs extend thin processes throughout their glomerular targets. In contrast, *Dscam* mutant fibers often terminate as intensely stained spatially restricted and condensed structures (arrows).

project into the CNS along the labial nerve frequently terminated not within the antennal lobe, but in regions surrounding it and the suboesophageal ganglion (Figure 2E, arrow, and see below).

Defects in Targeting of Eight Different Classes of ORNs Fall into Three Phenotypic Groups

We determined the role of Dscam in the targeting of eight different classes of ORNs: those expressing odorant receptors Or22a, Or23a, Or47a, and Or47b in the antenna (Figures 3 and 6); in those antennal neurons of unknown odorant receptor expression profile that are labeled in the GH298 enhancer trap line (Stocker et al., 1997) (hereafter referred to as GH298 neurons [Figure 3]); and maxillary palp neurons expressing Or46a, Or59c, and Or71a (Vosshall et al., 2000) (Figure 7). Targeting of different subclasses of ORNs were visualized by fusing the promoter regions of different ORs to Gal4 (Vosshall et al., 2000) and driving expression of a membrane-targeted version of GFP, UAS-mCD8-GFP, which highlights axons along their entire length, or of UAS-nsyb-GFP, which labels presynaptic terminals.

To assess targeting of different classes of ORNs, it is important to appreciate that about 90% of the antennal ORNs and all of the maxillary palp ORNs target to both an ipsilateral and contralateral target in equivalent positions in each antennal lobe (Stocker et al., 1990). That is,

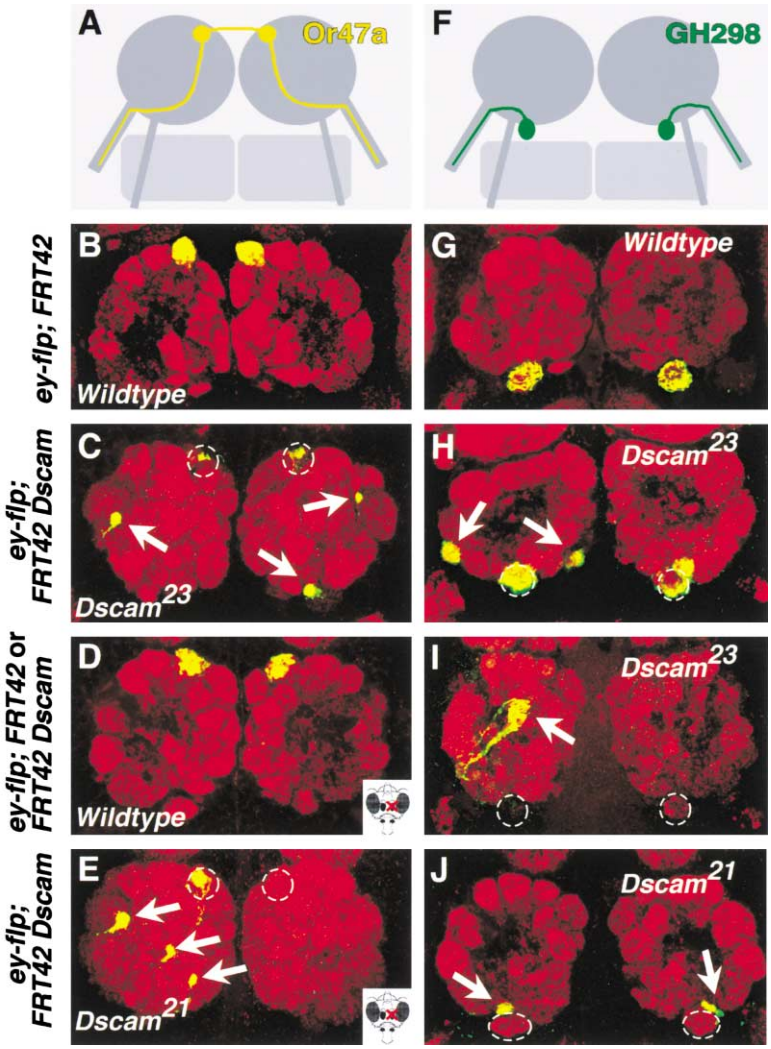

Figure 3. *Dscam* Mutant Or47a and GH298 Axons Target to Incorrect Glomeruli in the Ipsilateral Antennal Lobe

Left (A–E) and right (F–J) columns show the analysis of Or47a and GH298 projections, respectively. Cartoon representations of the projections of Or47a and GH298 axons are shown in panels (A) and (F). In all preparations, dorsal is up, and both the left and right antennal lobes are shown. Clones were generated as shown in Figure 2A. Ectopic termination sites are indicated by the arrows. Regions circled with white dashed lines represent the approximate boundaries of the cognate glomerulus for the class of ORNs being analyzed. (B) Targeting of wild-type Or47a axons to their appropriate glomeruli is shown. (C) Targeting defects in *Dscam* mutant Or47a axons innervating a wild-type target. (D and E) The left antenna was severed (indicated by icon in the lower right), and labeled terminals are from axons in the right antenna only (see text). (D) Note axon innervation of the left antennal lobe and innervation by the branch to the glomerulus on the right antennal lobe in wild-type. (E) *Dscam* mutant Or47a axons from the left antenna primarily mistarget in the ipsilateral antennal lobe (for quantification, see Figure 4A and 4B). (G) GH298 axons target to the ventrally located V glomerulus. These neurons do not extend contralateral branches (data not shown). (H–J) Dscam mutant GH298 axons projecting into a wild-type target. (H) These neurons frequently terminate at inappropriate locations in the ventral antennal lobe. (I) In other cases, GH298 axons do not turn ventrally after entering the lobe and terminate in more central and dorsal regions of the lobe. (J) Although fibers often turn ventrally and project to the V glomerulus, they frequently fail to enter it (arrows).

a single axon projects into a glomerulus in the ipsilateral lobe, and a branch then extends from it, dorsally across the midline, and terminates in a glomerulus in an equivalent position on the contralateral side (Figure 1B). Hence, to simplify the analysis of targeting defects in some experiments, we sought to determine the projection from only one antenna. To do this, single antennae from newly eclosed flies were removed, and neuronal projections from them were allowed to degenerate over a period of 7 days. This treatment does not affect the projections from the remaining antenna to either the ipsilateral or contralateral lobes (Vosshall et al., 2000). As a result, adult antennal lobes innervated by axons from a single antenna could be analyzed (Figures 3D, 3E, 6D–6F, and 6J–6L).

ORNs can be divided into three groups based on their *Dscam* mutant phenotypes. One group shows marked mistargeting of axons in the antennal lobe as they project toward their targets on the ipsilateral side (Figure 3). Another group leads to defects in innervation of the contralateral target glomerulus (Figure 6). This includes a reduction in branches and mistargeting to ectopic sites in the contralateral antennal lobe. And finally, the maxillary palp ORNs mistarget to inappropriate neuropil encountered along their path to the antennal lobe (Figure 7). We discuss each class separately in the following sections.

Dscam Mutant Or47a and GH298 Axons Project to Incorrect Targets in the Ipsilateral Antennal Lobe

We initially assessed the projections of Or47a ORNs to DM3, a glomerulus in the dorsal region of the antennal lobe (Figures 3A–3E). In wild-type, as Or47a axons exit the antennal nerve they spread out and project across the surface of the antennal lobe and, therefore, encounter numerous glomeruli prior to converging onto DM3 (Figures 3A and 3B). Strong Or47a mistargeting defects were observed in all three *Dscam* alleles examined (Figures 3C, 3E, and 4B). The penetrance of the phenotype in $Dscam^{21}$ is 100% with variable expressivity (on average about half of the mutant axons terminated in their correct glomerulus). The penetrance and expressivity of $Dscam^{23}$ and $Dscam^{33}$ were slightly less severe. Mutant Or47a axons preferentially mistarget to ventral, medial, and dorsal regions of the lobe, largely reflecting the distribu-

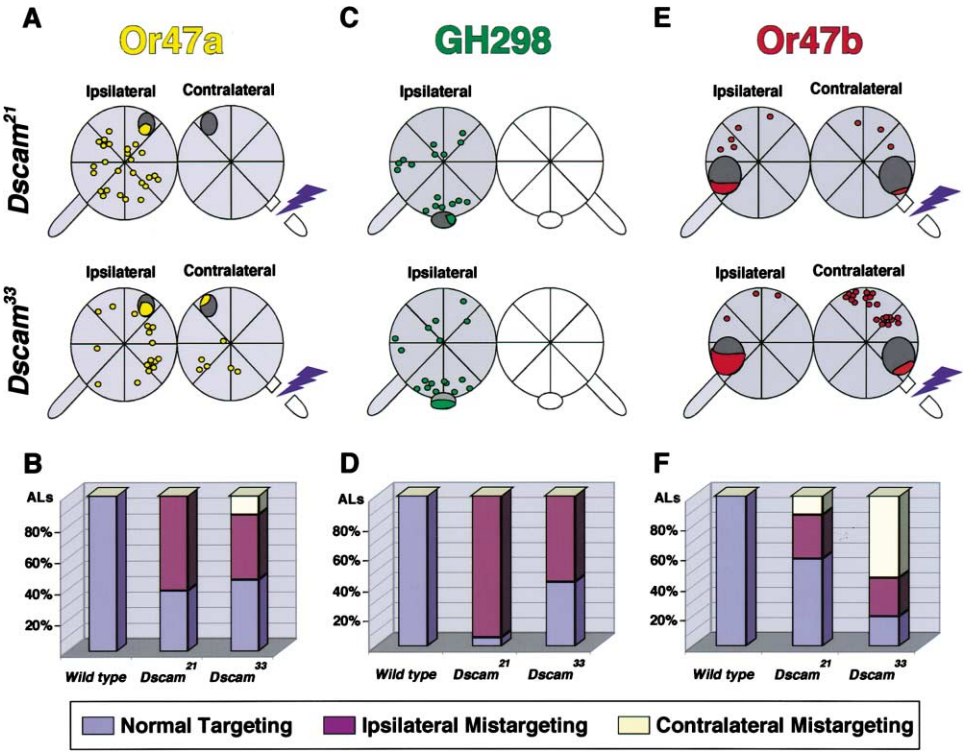

Figure 4. *Dscam* Mutant ORNs Mistarget to Different Sites in the Ipsilateral and Contralateral Antennal Lobes

(A and B) Or47a, (C and D) GH298, and (E and F) Or47b targeting defects in $Dscam^{21}$ and $Dscam^{33}$ are summarized. Ipsilateral and contralateral targeting for Or47a and Or47b axons was mapped in animals in which one antennal nerve was severed (jagged blue icon), allowing for assessment of targeting of mutant fibers from only one antenna. Between 20 and 30 brains were analyzed for each ORN subclass and genotype. Dorsal is up, and the midline separates the two lobes. (A and E) The sites of innervation of Or47a axons and Or47b from the left antenna are summarized schematically. The dark gray circles indicate the position of the cognate glomerulus. The small circles indicate targeting to ectopic locations, and the colored shading within cognate glomeruli represents an approximation of the extent of normal targeting. Or47a axons frequently innervate abnormal locations on the ipsilateral side as well as the cognate glomerulus. Targeting to either cognate or ectopic sites in the contralateral lobe was less frequent. (E) Targeting to the contralateral lobe for Or47b was more common. (C) As wild-type GH298 axons do not branch, targeting defects were assessed in animals with both antennal nerves intact. Dorsally mistargeted GH298 axons in *Dscam* mutant clones terminate on the ipsilateral side; they do not project contralaterally. The open circle at the bottom of the right antennal lobe in the GH298 analysis indicates that the glomerulus is not innervated by a contralateral branch. In (A), (C), and (E), antennal lobes contained one to two mistargeting sites on average. (B, D, and F) Mistargeting was quantified as indicated.

tion of Or47a fibers as they project dorsally toward DM3 (Figures 4A and 4B). Typically, mutant Or47a axons converge onto two to four ectopic sites. Most mistargeting was seen in the ipslateral lobe, although some mutant axons projected past their appropriate targets in both lobes and terminated ventrally on the contralateral side (Figures 4A and 4B).

GH298 targeting is also disrupted by *Dscam* mutations (Figures 3F–3J). In wild-type, as GH298 axons enter the antennal lobe, they turn ventrally to innervate the V (ventral-most) glomerulus. In about half the samples (in all three alleles examined), mutant axons leave the nerve, turn ventrally as in wild-type, and innervate ectopic positions within the ventral region of the antennal lobe (Figure 3H; Figures 4C and 4D). In the remaining preparations, GH298 mutant axons do not turn ventrally and terminate more dorsally (Figure 3I), typically, in more central and lateral regions of the lobe. In 20% of the preparations, none of the *Dscam* mutant GH298 fibers innervated the correct target (Figure 3J).

In summary, both Or47a and GH298 ORN subclasses show strong mistargeting phenotypes as they project toward their targets. Axons that fail to innervate their correct targets do not show an appreciable preference for specific alternative glomeruli.

The Fine Structure of Individual *Dscam* Mutant Or47a and GH298 Axon Terminals within Both Ectopic and Cognate Glomeruli Is Abnormal

To visualize the targeting behavior of individual Or47a and GH298 *Dscam* mutant axons, we generated small clones using FLP recombinase under the control of the heat shock-inducible promoter hsp70 (Figure 5). Single *Dscam* mutant Or47a axons exit the antennal nerve and often terminated in abnormal locations (Figures 5B and 5C). *Dscam* mutant Or47a terminals that reached their appropriate glomerulus failed to elaborate the network of thin arbors characteristic of wild-type terminals (compare Figure 5D to 5E and 5F). As the number of mutant fibers innervating the glomerulus increased, Or47a terminals remained largely restricted to the region adjacent to the axon entry site (data not shown). Branches ex-

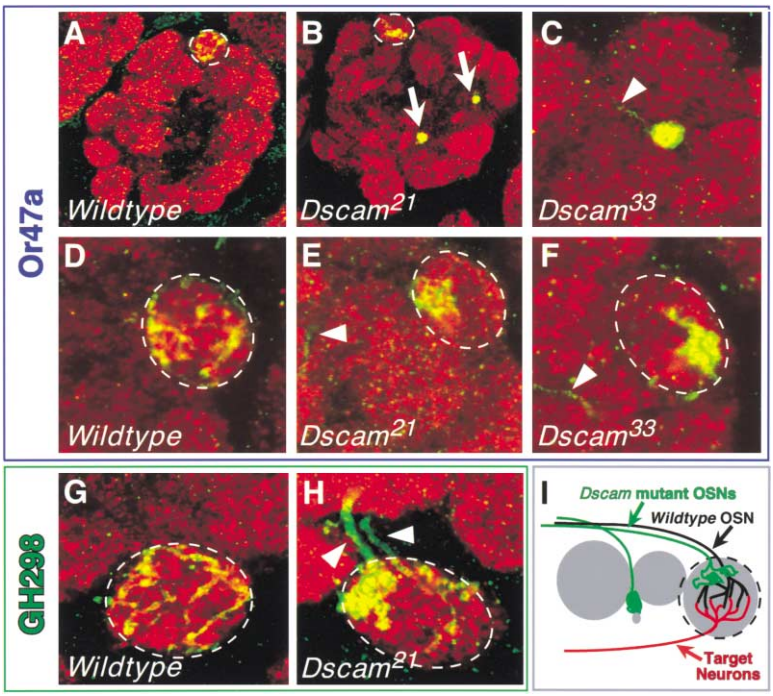

Figure 5. Single *Dscam* Mutant Fibers Mistarget and Have Abnormal Terminal Morphology

Single *Dscam* mutant ORNs or small numbers of mutant ORNs (<5) were generated by heat shock-induced mitotic recombination. Or47a (A–F) and GH298 (G and H) were examined. Single *Dscam* mutant Or47a axons (B and C) mistarget (arrows indicate ectopic termination sites) in the antennal lobe and appear to terminate between glomeruli (see schematic in [I]). Single axons are indicated with an arrowhead in (C). Single wild-type ORNs shown for Or47a (A and D) and GH298 (G) typically branch extensively throughout the target glomerulus. *Dscam* mutant Or47a terminals (B, E, and F) and GH298 (H) innervating the appropriate target glomeruli (demarcated by dashed lines) did not extend processes throughout the glomerulus but remained restricted to small domains. In some cases (F), intense spatially restricted staining within the glomerulus was observed. The V glomerulus in H is innervated by two mutant fibers (arrowheads). (I) Schematic representation of wild-type and *Dscam* mutant ORNs in ectopic and normal targets. Wild-type ORNs (black) form numerous thin branches within the appropriate target glomerulus. The dendrites of target neurons (red) are also highly branched. *Dscam* mutant fibers (green) that target to the appropriate glomerulus did not extend throughout it but largely remain as intensely stained clusters in subdomains of the glomerulus. Ectopic terminals were typically intensely stained. They are located between glomeruli and often are associated with clusters of nc82-stained processes, presumably from projection neurons, local interneurons, or both. Neuropil is indicated by gray staining.

tending from mutant fibers terminating either in ectopic locations or within the cognate target glomerulus were not observed (see below). Both ectopic targeting and defects in the morphology of GH298 terminals within the V glomerulus were also seen for single *Dscam* mutant GH298 axons (compare Figure 5G to 5H). The differences in the appearance of *Dscam* mutant terminals in ectopic and normal target glomeruli to wild-type terminals is schematically summarized in Figure 5I. These data indicate that Dscam is required to form or maintain normal synapse morphology within the appropriate glomerulus.

Dscam Is Required for Formation and Targeting of Contralateral Branches in Or47b, Or22a, and Or23a ORNs

We tested the *Dscam* requirement for targeting of two other ORNs that connect to dorsal glomeruli, Or22a (Figures 6A–6F) and Or23a (data not shown). In wild-type, these ORNs terminate in glomeruli that lie just medial and lateral to the glomerulus innervated by Or47a. Surprisingly, both Or22a and Or23a target normally in all three *Dscam* alleles tested (e.g., Figure 6C). Hence, different ORNs use different targeting strategies. Further analysis of these projections in *Dscam* mosaic animals in which one antenna was ablated revealed that, although targeting to their correct ipsilateral glomerulus was unaffected, both classes of ORNs showed a marked reduction in branches to the contralateral antennal lobe (e.g., Figures 6E and 6F). Interestingly, *Dscam* mutant Or47a axons that innervated DM3 also frequently fail to extend a contralateral branch (see Figure 3E). In some cases, they target to incorrect locations on the contralateral antennal lobe (Figures 4A and 4B).

To determine whether ORNs that normally terminate ventrally also show defects in contralateral branching, we assessed the targeting of Or47b axons to the VA1 l/m glomerulus (Figures 6G–6L). VA1 l/m is a large glomerulus and is encountered by ORNs immediately upon exiting the antennal nerve and entering the antennal lobe (Figures 6G and 6H). VA1 l/m was innervated by *Dscam* mutant Or47b axons in all samples, although mistargeting to dorsal regions was frequently observed (Figure 6I). Examination of projections in animals in which the one antenna was removed revealed that there were marked deficits in contralateral branches. The branching defects were most severe in $Dscam^{21}$ (Figure 6L). In all three alleles, however, mistargeting is also seen in more dorsal regions and in the contralateral lobe (Figures 6K, 4E, and 4F). It is not known whether these are axons that have failed to terminate within VA1 l/m or whether they are branches that have extended from VA1 l/m and targeted inappropriately.

In summary, Dscam is required for contralateral branch formation in the ORN subclasses Or22a, Or23a, Or47a, and Or47b. Lee and coworkers (Wang et al., 2002) previously observed defects in guidance of axon branches in mushroom body neurons. The phenotype described here for ORNs is different, as in many cases branches are missing. In addition to being required for branching, Dscam is also required for correct targeting in the contralateral antennal lobe for both Or47a and Or47b ORNs. That mistargeting is independent of branching defects is underscored by the strong mistargeting defects in GH298

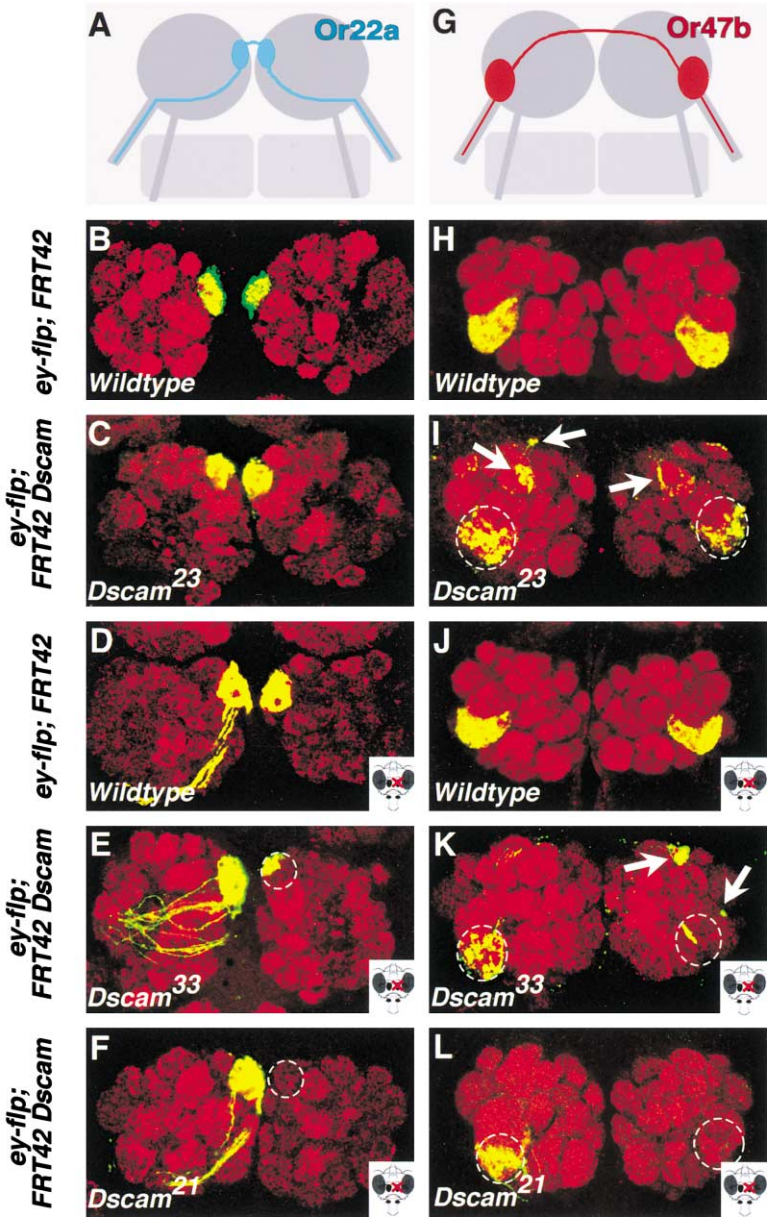

Figure 6. Dscam Is Required for Formation and Targeting of Contralateral Branches in Or22a and Or47b Neurons

(A and G) Schematic representation of projections of Or22a and Or47b are shown. Or22a and Or47b wild-type (B, D, H, and J) or *Dscam* mutant (C, E, F, I, K, and L) axon projections into a wild-type target are shown. The genotypes are indicated on the left. (D–F, J, and K) Removal of the left antenna (indicated by the icons on the lower right) reveals the innervation pattern from the right antenna. Note equal labeling from axons (right lobe) and branch (left lobe) in wild-type controls (D and J). The cognate glomeruli are indicated by circles with dashed lines (E, F, I, K, and L). (A–F) Targeting defects are not seen in Or22a axons. Removal of the left antenna showed a deficit (E) or lack (F) of innervation by contralateral branches. Compare to wild-type ablation in (D). (G–L) Targeting and branching defects were seen in Or47b *Dscam* mutant fibers. (I) Patchy innervation in the cognate glomerulus and ectopic targeting in more dorsal regions was observed. (K) While most Or47b fibers terminate in the cognate glomerulus as they enter the lobe, processes also extended into and terminated at ectopic sites and in the cognate glomerulus on the contralateral side. (L) Or47b fibers frequently fail to extend a branch. The marker in (D)–(F) is UAS-mCD8-GFP, which stains axons and terminals. Marker in all other panels was UAS-nsyb-GFP, which stains terminals only.

axons that do not branch in wild-type and mistargeting of Or47a to regions of the antennal lobe that are encountered prior to branching.

Dscam Mutant ORNs from the Maxillary Palps Mistarget to Neuropil Outside the Antennal Lobe

As the antennal nerve runs directly from the antenna to the antennal lobe, ORNs from the antenna are not presented with alternative targets prior to entering the target region. To assess whether targeting errors in ORNs resulting from loss of Dscam are restricted to the antennal lobe, we assessed the projections of three different classes of maxillary palp ORNs, Or46a, Or59c, and Or71a, which extend through the suboesophageal ganglion prior to entering the antennal lobe (Figures 7A, 7B, 7E, 7F, 7I, and 7J). Mutant *Dscam* ORNs of all three classes frequently terminated upon entering the ventral CNS before reaching the antennal lobe (Figures 7M and 7N), either immediately prior to entering the suboesophageal ganglion or upon exiting it, just ventral to the antennal lobe (Figures 7C, 7D, 7G, 7H, 7K, and 7L). Importantly, these mutant ORNs do not stop prematurely within the labial nerve but terminate upon encountering neuropil and forming a structure with the appearance of a glomerulus within it, arguing that this phenotype does not simply reflect defects in axon outgrowth. For Or46a and Or71c ORNs, mutant fibers coalesce to form a single glomerulus-like structure that stains with the neuropil marker nc82 (Figures 7D and 7L). In some cases, two glomerulus-like structures containing terminals of Or59c were seen. Hence, given the opportunity to terminate in a neuropil other than the

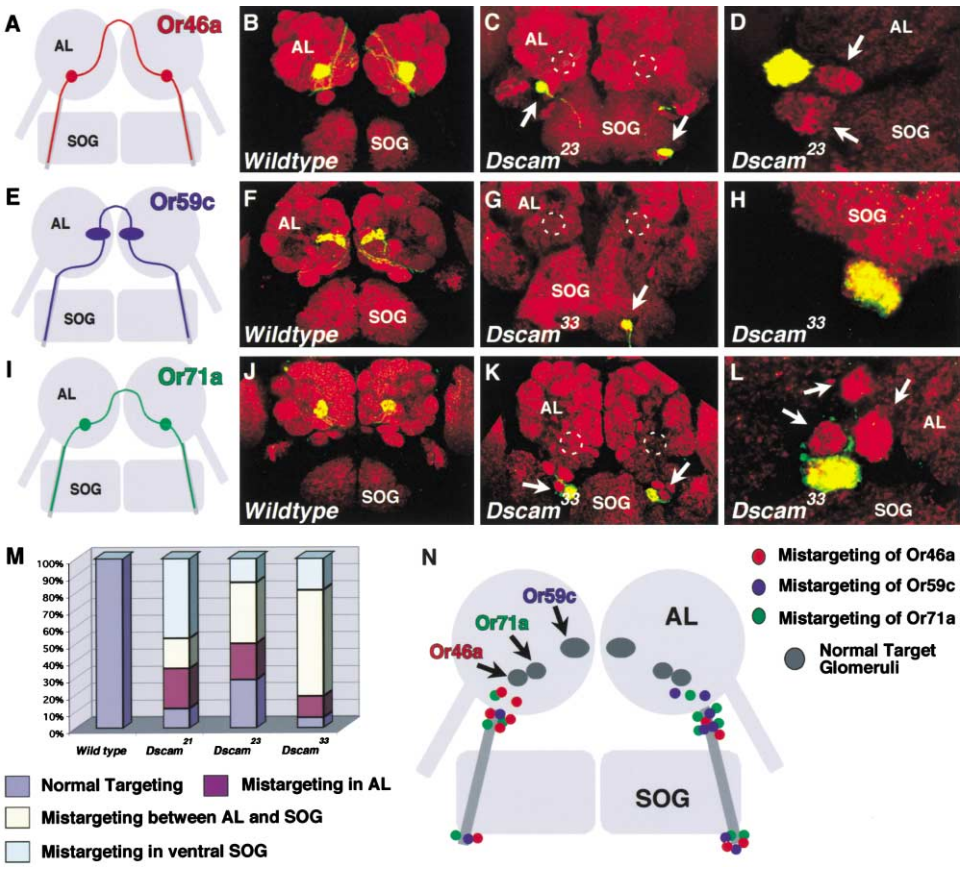

Figure 7. *Dscam* Mutant ORNs from the Maxillary Palps Segregate from Other Maxillary Palp ORNs and Induce Ectopic Glomeruli Outside the Antennal Lobe

Wild-type maxillary palp ORNs extend along the labial nerve through the suboesophageal ganglion (SOG), terminate in glomeruli located in the ventral medial region of the antennal lobe (AL), and extend branches contralaterally. This is shown for three different classes of maxillary palp ORNs, Or46a (A and B), Or59c (E and F), and Or71a (I and J). (A, E, and I) Schematics and (B, F, and J) UAS-nsyb-GFP-labeled terminals in wild-type. All mutant phenotypes in remaining panels were visualized with UAS-mCD8-GFP. (C, G, and K) Mistargeting to ectopic locations ventral to the suboesophageal ganglion and between the suboesophageal ganglion and the antennal lobe are seen in all three classes of maxillary palp axons (arrows). The dashed circles indicate the approximate location of the glomerulus innervated by wild-type axons. The arrows indicate aggregated terminals outside the antennal lobe. (D and L) High-magnification views of terminals of Or46a (D) and Or71a (L) show terminals segregated into discrete clusters adjacent to additional ectopic "glomeruli" (arrows) between the suboesophageal ganglion and antennal lobe. Preliminary evidence suggests that these are innervated by other subclasses of ORNs that are also mutant for *Dscam* (data not shown). (H) A high-magnification view of *Dscam* mutant fibers of the OR59c subclass which have terminated adjacent to the ventral region of the suboesophageal ganglion. (M) Mistargeting for the Or46a subclass for three different alleles analyzed is shown graphically. Between 15 to 20 animals were analyzed for each genotype. (N) The distribution of ectopic targeting for all three ORN subclasses analyzed in *Dscam*^{33} mosaics were plotted. For visualization purposes, about ten representative examples for each ORN subclass are shown.

antennal lobe, *Dscam* mutant ORNs from the maxillary palps frequently do so. As multiple ectopic glomerulus-like structures are seen with nc82 staining surrounding the ectopic glomerulus innervated by the labeled ORNs, it seems likely that different classes of maxillary palp *Dscam* mutant ORNs segregate into distinct ectopic glomeruli. Hence, *Dscam* acts in maxillary palp ORNs to prevent targeting to an inappropriate neuropil.

Discussion

Dscam plays a complex role in regulating the formation of specific connections in the fly olfactory system. In the absence of Dscam, two classes of antennal ORNs, Or47a and GH298, project into the antennal lobe, as they do in wild-type, but terminate at ectopic sites they encounter as they project to their cognate glomeruli. That Dscam prevents inappropriate targeting is underscored by the robust mistargeting of three classes of maxillary palp ORNs to neuropil outside the antennal lobe. In addition, ORN axons that reach the correct glomerulus do not elaborate a normal terminal region. They fail to extend thin processes throughout the cognate glomerulus as in wild-type and remain tightly segregated in local domains within the glomerulus. All ORNs studied that branch in wild-type to the contralateral glomerulus frequently fail to do so in *Dscam* mutants. It seems likely that defects in branching result from abnormalities in the interactions between ORNs and their cognate ipsilateral glomeruli. For some ORNs, branches target accurately to their cognate glomeruli on the contralateral antennal lobe, whereas in others they terminate in inappropriate

locations. While there are differences in *Dscam* phenotypes in different ORNs, as well as their penetrance and expressivity, these observations support a critical role for Dscam in mediating interactions between growth cones and neuropil within potential target regions.

Are alternative forms of Dscam required for targeting? In recent studies, we sought to assess whether expression of a single form of Dscam would rescue the targeting defects in specific olfactory receptor neurons. As expression in ORNs leads to a severe dominant phenotype with loss of glomerular structure (T.H. and S.L.Z., unpublished data), we have not been able to critically address the importance of multiple isoforms for targeting using this experimental approach. In future studies, the importance of alternative splicing in target selection will be assessed by analyzing loss-of-function mutants in which the number of alternative exons is reduced at the endogenous locus and by expressing additional isoforms of Dscam in ORNs.

It has been speculated that both ORNs and projection neurons express molecular labels that allow them to match-up in distinct glomeruli (Jefferis et al., 2001). Could the alternative forms of Dscam provide such labels? This is indeed a possibility, as Dscam is expressed on both ORNs and projection neurons during glomerular formation. That Dscam could act as a short-range attractant is consistent with the observation that mammalian Dscam proteins can bind to each other when expressed in transfected cells (Agarwala et al., 2001). Here, forms expressed on specific ORNs and the appropriate target projection neurons would selectively adhere to each other. Alternatively, Dscam could act as a short-range repellent. Projection neurons that extend dendrites selectively into only a single glomerulus may express a diverse set of Dscam isoforms, and different ORN subclasses express forms of Dscam that interact with isoforms expressed in dendrites of all projection neurons, except those in their cognate glomeruli. As a consequence, ORNs connect to their appropriate targets by being excluded from all other potential targets. Repulsion may be mediated by interactions between the same Dscam isoforms or between different isoforms; different isoforms may modulate the extent of repulsion between ORNs and target glomeruli, and hence, competitive interactions between ORN classes may contribute to specificity.

While Dscam is necessary for ORN targeting, it is clear that it is not the only ORN determinant regulating this process. Indeed, some ORN targeting is independent of Dscam (i.e., Or22a and Or23a), and in many cases, subclasses affected by *Dscam* mutations exhibit only partially penetrant phenotypes. This may reflect the overlapping function of other Dscams (i.e., Dscams 2–4; these Dscams do not come in multiple forms) that are expressed within the olfactory system (J.C.C., M.L.V., and S.L.Z., unpublished data) or the activity of redundant pathways utilizing other cell surface recognition molecules. Indeed, other targeting proteins, such as N-cadherin (Lee et al., 2001) and Flamingo (Lee et al., submitted), contribute to targeting of some but not all classes of ORNs (T.H. and S.L.Z., unpublished data). These studies allude to a complex combinatorial mechanism regulating olfactory receptor neuron targeting in *Drosophila*. The availability of markers for different neurons exhibiting different targeting specificities within a common ganglion provides a unique opportunity to explore the mechanisms regulating the formation of diverse patterns of synaptic connectivity.

Experimental Procedures

Isolation and Characterization of Additional *Dscam* Alleles

Fly stocks were maintained in standard medium at 22°C unless stated otherwise. Chemical mutagenesis was performed using ethyl methane sulfonate under standard conditions (Ashburner, 1989; Grigliatti, 1986). Twenty-two *Dscam* alleles were obtained. The strength of different alleles was determined by lethality and embryonic phenotypes as assessed in heteroallelic combinations and over a deficiency uncovering the Dscam locus [*Df(cos2)*]. For the studies reported here, we used the strong alleles $Dscam^{21}$, $Dscam^{23}$, and $Dscam^{33}$. For these alleles, no protein was detected on a Western blot with an antibody to the C terminus or in immunostaining of embryos with the N-terminal antibody.

Markers for Different Subsets of ORNs

To label a subset of ORNs, we used the following promoters fused to Gal4: Or22a, Or23a, Or46a, Or47a, and Or47b (Vosshall et al., 2000); Or59c and Or71c (Y.F. and L.B.V., unpublished data). Axons innervating the V glomerulus were detected using the enhancer trap insertion GH298-Gal4 (Stocker et al., 1997). The reporters to visualize axons and synaptic terminals were UAS-mCD8-GFP (Lee and Luo, 1999) and UAS-nsyb-GFP (Estes et al., 2000). To visualize all ORNs in mosaics, the enhancer trap line Gal4-C155 (elav-Gal4; Lin and Goodman, 1994) was used. Projection neurons were visualized in Figure 1H with the enhancer trap line GH146-Gal4 (Stocker et al., 1997).

Genetic Mosaics

All genetic mosaics were generated using the MARCM system (Lee and Luo, 1999) with various Gal 4 drivers (see previous section) and FRT42 TubP-Gal80 on the second chromosome. For large clones in the antenna and maxillary palps, an *ey-FLP* insertion on the X chromosome was used (Newsome et al., 2000). For small clones and single-cell analysis, a *hsp70-FLP* transgene on the X chromosome was used (Golic and Lindquist, 1989). To visualize all ORNs, mosaics were generated in flies of the following genotype: *ey-FLP, elav-Gal4; FRT Dscam/FRT TubP-Gal80; UAS-mCD8-GFP*. To analyze the role of *Dscam* in identified subsets of ORNs, mosaics were generated in animals of the following genotype: *ey-FLP; FRT Dscam/FRT TubGal80; Or-Gal4 UAS-GFP. Or-Gal4* represents different drivers, as indicated in the previous section. Single-cell clones were obtained by heat shocking late third instar larvae (30 min at 37°C) of the following genotypes: *hsp70-FLP;FRT Dscam/FRT Gal80; Or47a-Gal4 UAS-mCD8-GFP* and *hsp70-FLP;FRT Dscam/FRT Gal80; GH298-Gal4, UAS-mCD8-GFP. GH298-Gal4* is a promoter fusion that shows the same glomerular specificity as GH298-Gal4 (Scott et al., 2001).

Immunohistology

Primary antibodies used for immunohistochemistry were rabbit anti-Dscam C-terminal (gift of C. Worby and J. Dixon) and N-terminal (Schmucker et al., 2000); rabbit anti-GFP (Molecular Probes); and nc82 (Stortkuhl et al., 1994). Secondary antibodies used were goat anti-rabbit F(ab)′ fragment coupled to Alexa-488 (Molecular Probes) and goat anti mouse F(ab)′ fragment coupled to Cy3 (Jackson Laboratories)

Immunostaining of brains of adult flies and pupae were carried out essentially as described in Van Vactor et al. (1991), with the following exceptions: (1) adult brains were fixed in 2% PFA for 90 min; and (2) for the dissection of the pupal brains, the pupal cases were open, 2% PFA was added, and the brains were allowed to fix for 10 min before further dissection in 2% PFA. The overall time of fixation in 2% PFA was 90 min. Fluorescent samples were analyzed using a Bio-Rad MRC 1024 confocal microscope.

In situ hybridization to detect Dscam mRNA was done in 40% pupal brains and antennae using digoxygenin-labeled RNA probes following the protocol for imaginal discs in Sullivan et al. (2000).

RT-PCR of Pupal Antennae

Six third antennal segments were dissected from pupae at ~30 hr after puparium formation, and total RNA was isolated from each antenna separately. Separate RT-PCR reactions were set up for each antenna. cDNAs were subcloned and sequenced. RT-PCR was performed largely as described in Schmucker et al. (2000).

Acknowledgments

We thank Richard Axel, Utpal Banerjee, Tom Clandinin, Eddy De-Robertis, Liqun Luo, and members of the Zipursky lab for comments on the manuscript. We are grateful to Reinhard Stocker for fly stocks and reagents and Karen Ronan for help with the manuscript. This work was supported by a postdoctoral fellowship from the Human Frontiers Science Program (T.H.), a predoctoral fellowship from the Gulbenkian Ph.D. Program in Biology and Medicine, and the Foundation for Science and Technology in Portugal (M.L.V.), and a postdoctoral fellowship from the Helen Hay Whitney Foundation (J.C.C.). S.L.Z. is an Investigator of the Howard Hughes Medical Institute.

Received: September 30, 2002
Revised: December 11, 2002

References

Agarwala, K.L., Ganesh, S., Tsutsumi, Y., Suzuki, T., Amano, K., and Yamakawa, K. (2001). Cloning and functional characterization of DSCAML1, a novel DSCAM-like cell adhesion molecule that mediates homophilic intercellular adhesion. Biochem. Biophys. Res. Commun. *285*, 760–772.

Ashburner, M. (1989). *Drosophila*: A Laboratory Manual (Cold Spring Harbor, NY: Cold Spring Harbor Laboratory Press).

Clyne, P.J., Warr, C.G., Freeman, M.R., Lessing, D., Kim, J., and Carlson, J.R. (1999). A novel family of divergent seven-transmembrane proteins: candidate odorant receptors in *Drosophila*. Neuron *22*, 327–338.

Elmore, T., and Smith, D.P. (2001). Putative Drosophila odor receptor OR43b localizes to dendrites of olfactory neurons. Insect Biochem. Mol. Biol. *31*, 791–798.

Estes, P.S., Ho, G.L., Narayanan, R., and Ramaswami, M. (2000). Synaptic localization and restricted diffusion of a Drosophila neuronal synaptobrevin-green fluorescent protein in vivo. J. Neurogenet. *13*, 233–255.

Flanagan, J.G., and Vanderhaeghen, P. (1998). The ephrins and Eph receptors in neural development. Annu. Rev. Neurosci. *21*, 309–345.

Gao, Q., and Chess, A. (1999). Identification of candidate Drosophila olfactory receptors from genomic DNA sequence. Genomics *60*, 31–39.

Gao, Q., Yuan, B., and Chess, A. (2000). Convergent projections of Drosophila olfactory neurons to specific glomeruli in the antennal lobe. Nat. Neurosci. *8*, 780–785.

Golic, K.G., and Lindquist, S. (1989). The FLP recombinase of yeast catalyzes site-specific recombination in the *Drosophila* genome. Cell *59*, 499–509.

Grigliatti, T. (1986). Mutagenesis. In *Drosophila*: A Practical Approach, D.B. Roberts, Ed. (Oxford: IRL press).

Huh, G.S., Boulanger, L.M., Du, H., Riquelme, P.A., Brotz, T.M., and Shatz, C.J. (2000). Functional requirement for class I MHC in CNS development and plasticity. Science *290*, 2155–2159.

Jefferis, G.S., Marin, E.C., Stocker, R.F., and Luo, L. (2001). Target neuron prespecification in the olfactory map of Drosophila. Nature *414*, 204–208.

Kohmura, N., Senzaki, K., Hamada, S., Kai, N., Yasuda, R., Watanabe, M., Ishii, H., Yasuda, M., Mishina, M., and Yagi, T. (1998). Diversity revealed by a novel family of cadherins expressed in neurons at a synaptic complex. Neuron *20*, 1137–1151.

Laissue, P.P., Reiter, C., Hiesinger, P.R., Halter, S., Fischbach, K.F., and Stocker, R.F. (1999). Three dimensional reconstruction of the antennal lobe in Drosophila melanogaster. J. Comp. Neurol. *405*, 543–552.

Lee, T., and Luo, L. (1999). Mosaic analysis with a repressible cell marker for studies of gene function in neuronal morphogenesis. Neuron *22*, 451–461.

Lee, C.H., Herman, T., Clandinin, T.R., Lee, R., and Zipursky, S.L. (2001). N-cadherin regulates target specificity in the *Drosophila* visual system. Neuron *30*, 437–450.

Lin, D.M., and Goodman, C.S. (1994). Ectopic and increased expression of Fasciclin II alters motoneuron growth cone guidance. Neuron *13*, 507–523.

Mombaerts, P., Wang, F., Dulac, C., Chao, S.K., Nemes, A., Mendelsohn, M., Edmondson, J., and Axel, R. (1996). Visualizing an olfactory sensory map. Cell *87*, 675–686.

Newsome, T.P., Asling, B., and Dickson, B.J. (2000). Analysis of Drosophila photoreceptor axon guidance in eye-specific mosaics. Development *127*, 851–860.

Schmucker, D., Clemens, J.C., Shu, H., Worby, C.A., Xiao, J., Muda, M., Dixon, J.E., and Zipursky, S.L. (2000). *Drosophila* Dscam is an axon guidance receptor exhibiting extraordinary molecular diversity. Cell *101*, 671–684.

Scott, K., Brady, R., Jr., Cravchik, A., Morozov, P., Rzhetsky, A., Zuker, C., and Axel, R. (2001). A chemosensory gene family encoding candidate gustatory and olfactory receptors in *Drosophila*. Cell *104*, 661–673.

Stocker, R.F., Lienhard, M.C., Borst, A., and Fischbach, K.F. (1990). Neuronal architecture of the antennal lobe in Drosophila melanogaster. Cell Tissue Res. *262*, 9–34.

Stocker, R.F., Heimbeck, G., Gendre, N., and de Belle, J.S. (1997). Neuroblast ablation in Drosophila P[GAL4] lines reveals origins of olfactory interneurons. J. Neurobiol. *32*, 443–456.

Stortkuhl, K.F., Hofbauer, A., Keller, V., Gendre, N., and Stocker, R.F. (1994). Analysis of immunocytochemical staining patterns in the antennal system of Drosophila melanogaster. Cell Tissue Res. *275*, 27–38.

Sullivan, W., Ashburner, M., and Hawley, R.S. (2000). *Drosophila* Protocols (Cold Spring Harbor, NY: Cold Spring Harbor Laboratory Press).

Tessier-Lavigne, M., and Goodman, C.S. (1996). The molecular biology of axon guidance. Science *274*, 1123–1133.

Van Vactor, D.L., Jr., Cagan, R.L., Kramer, H., and Zipursky, S.L. (1991). Induction in the developing compound eye of *Drosophila*: multiple mechanisms restrict R7 induction to a single retinal precursor cell. Cell *67*, 1145–1155.

Vosshall, L.B., Amrein, H., Morozov, P.S., Rzhetsky, A., and Axel, R. (1999). A spatial map of olfactory receptor expression in the *Drosophila* antenna. Cell *96*, 725–736.

Vosshall, L.B., Wong, A.M., and Axel, R. (2000). An olfactory sensory map in the fly brain. Cell *102*, 147–159.

Wang, F., Nemes, A., Mendelsohn, M., and Axel, R. (1998). Odorant receptors govern the formation of a precise topographic map. Cell *93*, 47–60.

Wang, J., Zugates, C.T., Liang, I.H., Lee, C.H., and Lee, T. (2002). *Drosophila* Dscam is required for divergent segregation of sister branches and suppresses ectopic bifurcation of axons. Neuron *33*, 559–571.

Winberg, M.L., Mitchell, K.J., and Goodman, C.S. (1998). Genetic analysis of the mechanisms controlling target selection: complementary and combinatorial functions of netrins, semaphorins, and IgCAMs. Cell *93*, 581–591.

Wu, Q., and Maniatis, T. (1999). A striking organization of a large family of human neural cadherin-like cell adhesion genes. Cell *97*, 779–790.

Yamakawa, K., Huot, Y.K., Haendelt, M.A., Hubert, R., Chen, X.N., Lyons, G.E., and Korenberg, J.R. (1998). DSCAM: a novel member of the immunoglobulin superfamily maps in a Down syndrome region and is involved in the development of the nervous system. Hum. Mol. Genet. *7*, 227–237.

Yu, T.W., and Bargmann, C.I. (2001). Dynamic regulation of axon guidance. Nat. Neurosci. Suppl. *4*, 1169–1176.